Chemical & Biomedical Engineering Faculty Publications

Chemical & Biomedical Engineering Department

11-6-2019

Periodic Operation of a Dynamic DNA Origami Structure Utilizing the Hydrophilic−Hydrophobic Phase-Transition of Stimulus-Sensitive Polypeptides

Marisa A. Goetzfried
Technische Universität München

Kilian Vogele
Technische Universität München

Andrea Mückl
Technische Universität München

Marcus Kaiser
Technische Universität München

Nolan B. Holland
Cleveland State University

Repository Citation

Authors

Marisa A. Goetzfried, Kilian Vogele, Andrea Mückl, Marcus Kaiser, Nolan B. Holland, Friedrich C. Simmel, and Tobias Pirzer

Periodic Operation of a Dynamic DNA Origami Structure Utilizing the Hydrophilic–Hydrophobic Phase-Transition of Stimulus-Sensitive Polypeptides

Marisa A. Goetzfried, Kilian Vogele, Andrea Mückl, Marcus Kaiser, Nolan B. Holland, Friedrich C. Simmel, and Tobias Pirzer

Dynamic DNA nanodevices are designed to perform structure-encoded motion actuated by a variety of different physicochemical stimuli. In this context, hybrid devices utilizing other components than DNA have the potential to considerably expand the library of functionalities. Here, the reversible reconfiguration of a DNA origami structure using the stimulus sensitivity of elastin-like polypeptides is reported. To this end, a rectangular sheet made using the DNA origami technique is functionalized with these peptides and by applying changes in salt concentration the hydrophilic–hydrophobic phase transition of these peptides actuate the folding of the structure. The on-demand and reversible switching of the rectangle is driven by externally imposed temperature oscillations and appears at specific transition temperatures. Using transmission electron microscopy, it is shown that the structure exhibits distinct conformational states with different occupation probabilities, which are dependent on structure-intrinsic parameters such as the local number and the arrangement of the peptides on the rectangle. It is also shown through ensemble fluorescence resonance energy transfer spectroscopy that the transition temperature and thus the thermodynamics of the rectangle-peptide system depends on the stimuli salt concentration and temperature, as well as on the intrinsic parameters.

1. Introduction

DNA nanotechnology utilizes DNA molecules both for the creation of static nano-architectures as well as for the realization of dynamic nanodevices or even macromolecular machines. Defining the latter as molecular-scale equivalents of macroscopic machines, they have been considered as a particular type of molecular device "in which the relative positions of the component parts can change as a result of some external stimulus."[1]

In particular the DNA origami technique has been shown to be an excellent tool to build well-defined macromolecular structures.[2–6] For this, hundreds of oligomeric DNA strands (the "staple strands") are hybridized to a long DNA "scaffold strand" to enforce folding of the scaffold into a desired shape.

One approach toward the implementation of machine-like behaviors in DNA origami structures[7] is based on the creation of molecular assemblies, in which multiple origami subunits are connected with each other via simple machine elements such as pivots or hinges.[8,9] When the subunits are further made to bind with each other through sufficiently weak interactions, which can be reversibly switched by external stimuli,[10–13] the structural components can change their relative positions, resulting in an overall conformational change.

The stimuli and energy sources for the operation of such devices can be quite diverse, for instance, DNA strand displacement processes,[14,15] binding of biomolecules through aptamers,[16] environmental changes (e.g., changes in salt concentrations[9,12] or physical stimuli such as temperature[13,17]), or electric[18,19] and magnetic fields.[20,21] In many cases, "switchability" has been introduced by appropriate chemical modifications of the devices. For instance, photoswitchable devices have been realized by utilizing the well-known *cis–trans* photoisomerization of azobenzene derivatives.[22,23] Other organic modifications were used to switch the conformation of DNA nanodevices by exploiting their hydrophobic interactions.[10,11,24–27] Recently, Vogele et al.[17] utilized thermoresponsive peptides to actuate an active plasmonic waveguide defined on a DNA origami structure

and Turek et al.[13] used a similar approach to actuate a DNA origami flexor.

These switchable devices could be utilized in nanotechnology for the development of more sophisticated machinery or even microscaled factories, but also for biomedical applications, responsive macromolecular assemblies are highly desirable. In the last years, DNA origami structures have been examined and developed for combined delivery and release systems.[16,28–33] In order to achieve this, several control mechanisms and stimuli need to be developed to fulfill the desired needs, for instance, for disease-related markers (e.g., microRNA) or for the specific pH in cancer tissue.

In the present work, we utilize the stimuli-responsive properties of elastin-like polypeptides (ELPs) to periodically switch the conformation of a rectangular DNA origami structure through two external stimuli, namely salt concentration and temperature. The DNA structure serves as the mechanical framework, while the ELPs are used as the decisive control elements that allow us to change the relative positions of the mechanical components of the structure on demand. When a specific stimulus is applied, ELPs can change from a hydrophilic to a hydrophobic state, as determined by whether it is below or above its transition temperature, T_t. We also demonstrate how the location and arrangement of the ELP control elements (further denoted as configuration) influences the performance, the conformational states, and the thermodynamics of our dynamic origami devices. Similar to proteins, our devices exhibit several conformational states which can be engineered by changing the configuration of the ELP modifications. The design also influences the thermodynamic behavior which becomes apparent through changes in T_t and cooperativity of the transition.

ELPs are synthetic peptides[34–36] consisting of repetitive sequences derived from the naturally occurring protein tropoelastin which is the precursor of elastin.[28] The canonical amino acid motif of ELPs is $(G\alpha GVP)_n$, where α can be any amino acid but proline and n denotes the number of pentapeptide repeats. In this work, canonical $(GVGVP)_{40}$ peptides, abbreviated as V40, but also peptides with a mixture of the GVGVP motif and the noncanonical GVGVAGVP motif were used. Both types of peptides undergo a fully reversible phase transition from a water-soluble hydrophilic state to a collapsed hydrophobic state when the sample is heated above the transition temperature T_t. The reported conformation of ELPs in their hydrophobic state is a β-spiral.[34] The T_t depends on various parameters such as the concentration and the type of electrolytes in the solute, ELP concentration and length, and the amino acid used for the variable position α. More hydrophobic amino acids result in a lower T_t, less hydrophobic α generate a higher T_t. This feature allows the specific design of T_t by using one specific amino acid or a combination of polar and nonpolar amino acids for α along the peptide. The incorporation of noncanonical motifs changes T_t in the same way. An isothermal phase transition can be triggered by changing, for instance, the environmental conditions through the addition of salt depending on the specific T_t of the peptides and is called the ΔT_t mechanism. Fundamentally, ELPs can be used as transducer to convert one form of energy into a second energy form.

Some decades ago, Urry classified ELP-based molecular machines in three categories.[37,38] A device that operates by thermally driven contraction (folding) on raising the temperature is called a zero-order molecular machine of the T_t type. Any other device, where mechanical motion (folding) is involved, is called first-order molecular machine of the T_t type. If a device converts energy not involving mechanical force, it is called a second-order molecular machine of the T_t type; an example would be the reduction of nicotinamide moieties, which are bound to ELP amino acid side chains, resulting in the protonation of ELP carboxylate groups. In principle, only one ELP sequence would be sufficient to perform all three kinds of energy conversions. Because of these properties and the reversibility of the phase transition, ELPs represent an attractive alternative for nonpolar molecules such as cholesterol or long-chained alkanes[26,27] for the modification of DNA origami structures, as it is not necessary to use surfactants to alter the hydrophobic effect or to reconfigure a structure.[10,11] However, because of the contour length of commonly used ELPs and the high water content of ELP coacervates diverse hydrophobic interactions and effects might be evolved; therefore devices utilizing ELPs require a thorough design and analysis.

The term "hydrophobicity" describes various phenomena and interactions involving nonpolar molecules and interfaces in an aqueous environment. The range of the hydrophobic effect has been reported to be up to several micrometers, whereby only the short-range part of this interaction (<10 nm) has been called the "true" hydrophobic effect.[39] Instead of a defined bond, the interaction is dominated by the hydration of nonpolar molecules and interfaces. For the long-range attraction, various mechanisms such as bubble coalescence play a role. Because of this nonlocal nature of the hydrophobic effect, the fabrication and folding of a DNA nanodevice using hydrophobic molecules is not just a straightforward mechanical task. In fact, actuation of origami structures using intraorigami hydrophobic interactions is somewhat reminiscent of protein-folding processes, and we therefore utilized principles taken from polymer physics and protein folding to guide the design of the ELP-modified DNA rectangle. Early models of protein folding stated that hydrogen bonding is responsible for secondary structure formation in proteins. However, experiments showed that hydrogen bonding and other local interactions only are strong determinants for the folding of short peptides, but weaker determinants for the structure of globular proteins. A popular and more advanced model to describe protein folding is the HP lattice model proposed by Dill and co-workers.[40] In this model, the primary sequence is modeled as a chain of hydrophobic (H) and polar (P) monomers and folding occurs by embedding these monomers into a 2D or 3D lattice. The more H monomers are adjacent on this lattice the lower is the free energy of the chain. In particular, for peptides the model states that rather the side chains and their solvation instead of the backbone and its torsion angles determine the structure. From a general point of view, the folding code thus is more of a solvation code and less an encoding of torsion angles along the peptide polymer. This automatically implies that multiple interactions will contribute to the final structure, its thermodynamics, and kinetics of folding.[41,42] In the present study we designed the configurations of the ELP control elements by following these established principles for polymer and peptide folding. The DNA rectangle stands for the "backbone," whereas the peptides represent the "side chains."

2. Results and Discussion

2.1. Device Configuration and Periodic Thermal Actuation

The underlying mechanical framework used for our peptide-actuated nanodevice was provided by a flexible twist-corrected DNA origami rectangle (90 nm × 60 nm),[10,11] which comprised a central hinge region to promote rotational motion of the two leaves of the structure around the hinge axis (**Figure 1**a; Figure S9, Supporting Information).

For the attachment of ELPs on a grid defined on the origami structure, specific staple strands were modified and elongated with sequences complementary to those of the DNA-linker molecules L_{DNA} covalently linked to the ELPs (for illustration, see Figure 1b,c and also Figure S3 and Table S1 in the Supporting Information). In order to be able to specify individual ELP configurations, we labeled the rows of the grid with capital letters from A to E, and the columns with numbers 1 to 7. The hinge was constructed in row C via the insertion of two thymidines into the local staples. The nominal separation between neighboring rows is ≈10 nm, while adjacent columns have a distance of ≈11 nm. Due to constraints by the scaffold routing of the DNA origami structure, column 4 had to be shifted by ≈6 nm (see Figures S8–S11 in the Supporting Information), which was not observable, however, in atomic force microscopy (AFM) imaging (see Figure 1d). The number and arrangement of the binding sites were varied in clusters of up to 14 per leaf consisting of two rows with up to seven sites each (see Figure S1 in the Supporting Information). Example

configurations are shown in Figure 1, such as the ABDE345 with six ELPs attached to the center of each leaf.

In order to determine the binding yield of L_{DNA}–V40 to the binding sites on the hinged rectangles, we used AFM imaging and counted the visible peptides for the configurations ABDE345 (Figure 1d), ABDE1267, and BD345 (Section S2.3, Supporting Information). Due to the mirror symmetry of these configurations, we determined the binding yield per leaf. For ABDE345 comprising six binding sites per leaf, we found that in about 37% of the structures, all six binding sites were occupied by L_{DNA}–V40, while 23% of the structures carried five L_{DNA}–V40. Figure 1d shows the binomial distribution of the determined binding yield, with a total probability of 76% that one leaf is functionalized with at least four peptides (see Section S2.3, Supporting Information). Due to the flexibility of the rectangle-bound peptides, it was only possible to determine the number of peptides per leaf, but not the exact position of each V40. We therefore cannot exclude a potential position dependence of the binding yield per "binding site."[43,44]

We first studied reversible opening and closing of ABDE345 and the other ELP-origami constructs in bulk solution using Förster resonance energy transfer (FRET) between the fluorescent dyes Atto 532 and Atto 647N (Figure 1a; Section S3.1, Supporting Information), which were incorporated into the structure using dye-modified staples. Origami motion was stimulated by the cyclic variation of the sample temperature between 10 and 55 °C in folding buffer (FB, 40×10^{-3} M Tris-acetate, 10×10^{-3} M ethylenediaminetetraacetic acid (EDTA) and 20×10^{-3} M $MgCl_2$, with additional 1.0 M NaCl). As can be
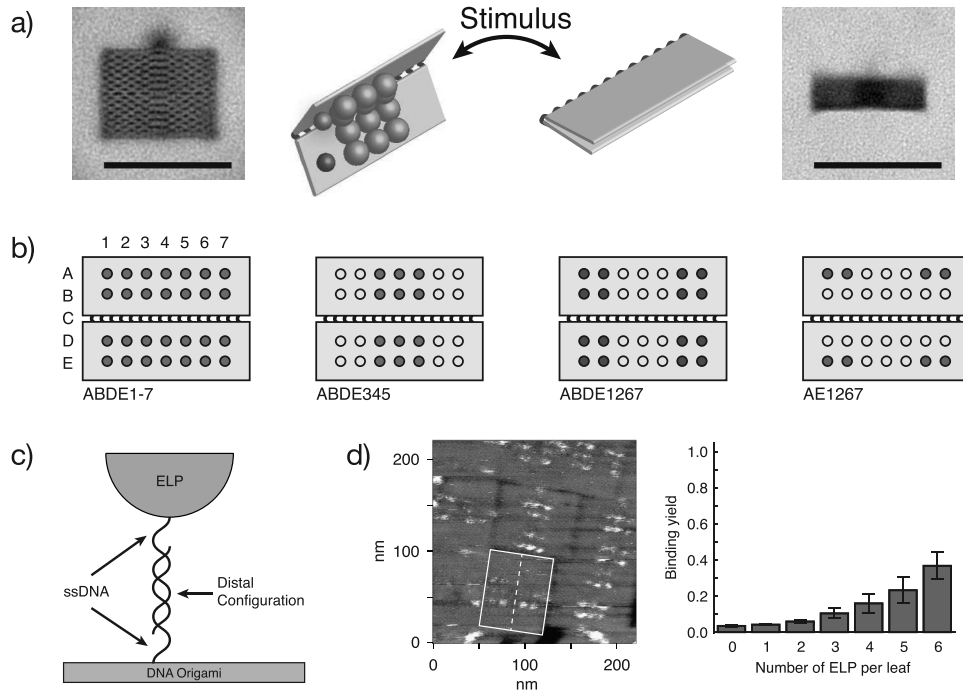

Figure 1. DNA origami design and ELP configuration. a) Class-averaged TEM images of an open rectangle (left) and a closed rectangle (right). Center: Illustration of the working principle and the rectangle design with ELPs (orange spheres) and dyes (red and blue). Scale Bar: 100 nm. b) Graphical representation of four exemplary ELP-rectangle configurations. c) Illustration of the binding site design in distal configuration. d) Left: Representative AFM image of the rectangle with attached ELPs in ABDE345 configuration. Right: Binomial distribution of the ELP-occupied binding sites per leaf. The given uncertainties are standard deviations.
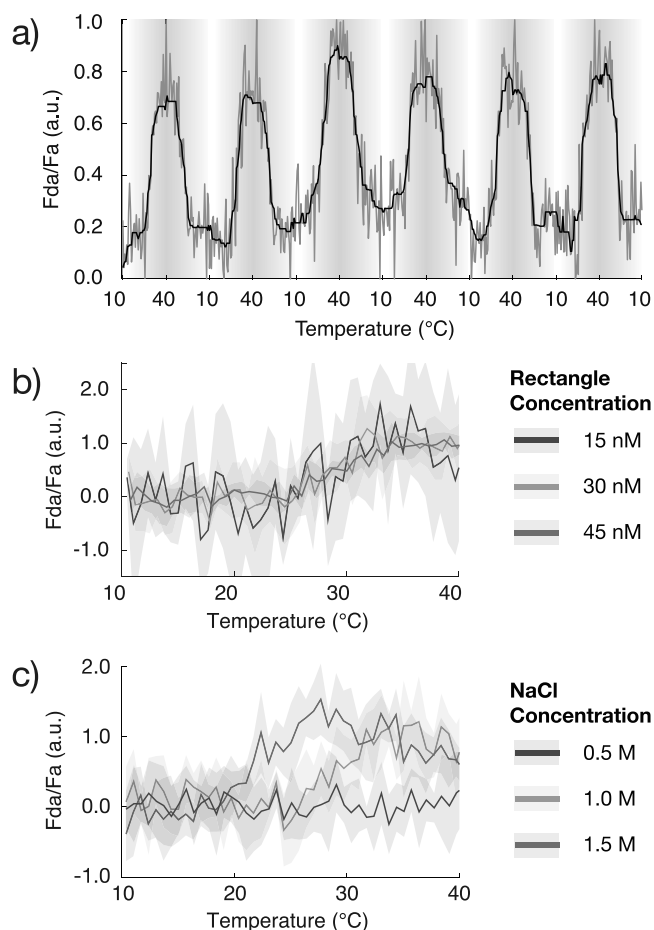
Figure 2. Periodic actuation of the rectangle ABDE345. a) Normalized FRET signal (raw data in gray and 15-points median filtered in black) for six heating and cooling ramps in the range between 10 and 40 °C. b) Normalized FRET signal for three rectangle concentrations, 15×10^{-9} M (blue), 30×10^{-9} M (green), and 45×10^{-9} M (red). Solid lines depict the averaged curve of the heating curves from temperature oscillation experiments with 1 M NaCl. Light-colored areas indicate the standard deviation for each point. c) Normalized FRET signal for three NaCl concentrations, 0.5 M (blue), 1.0 M (green), and 1.5 M (red). Solid lines depict the averaged curve of the heating curves. Light-colored areas indicate the standard deviation of each point. The corresponding cooling curves can be seen in the Data overview file in the Supporting Information.

seen in **Figure 2**a, the FRET signal reversibly follows the temperature variation, indicating successful and repeated conformational switching of the devices.

The temperature transition for the ABDE345 folding can then be determined by plotting the FRET signal versus temperature (Figure 2b,c). We found that the temperature transition is independent of the rectangle concentration (which only affects the signal-to-noise ratio, Figure 2b), while T_t can be systematically altered through a change in the NaCl concentration, which is shown in Figure 2c for FB with additional 0.5 M NaCl, 1.0 M NaCl, or 1.5 M NaCl.

The apparent signal decrease at high temperatures originates from the temperature dependence of the acceptor dye (see the Data overview file in the Supporting Information) and was fully reversible. For [NaCl] ≤ 0.5 M, no FRET signal was observed,

which indicates a transition temperature above 55 °C, whereas for [NaCl] ≥ 2 M, T_t was below 10 °C, resulting in a high FRET signal for all temperatures applied in the experiment (see Data overview file in the Supporting Information).

2.2. Intrastructure versus Interstructure Interaction

In a previous study performed on origami rectangles functionalized with cholesterol moieties, it was found that hydrophobic interactions can also promote dimerization of the structures,[10] which would also lead to a measurable FRET signal. In order to assess the propensity of ELP rectangles for intrastructure versus interstructure assembly (i.e., dimerization), we performed transmission electron microscopy (TEM) imaging. Instead of using temperature to control the state of the ELPs, we utilized NaCl concentration to permanently switch the V40 peptides either into their hydrophilic ([NaCl] = 0 M) or their hydrophobic state ([NaCl] = 3 M) before imaging the structures at room temperature. TEM image analysis was automated using MATLAB (see Section S2.4, Supporting Information). In **Figure 3**a, the results for the different ELP configurations are shown, with the monomer fraction in dark colors and the dimeric assembly fraction in light colors, at concentrations of 0 M NaCl (blue) and 3 M NaCl (red). We found that, irrespective of the salt concentration, roughly 20% of the ABDE345 configuration, but also ≈30% of the negative control without any V40, appeared to form dimeric assemblies. This points toward a measurement artifact most likely originating from the adsorption process and an overlap of the structures on the TEM grid (Figure 3b, right). We therefore assumed that samples with "measured" dimerization fractions on the order of or below ≈20–30% in reality are dimerization free (an exhaustive overview of the dimer fraction determined for all samples investigated can be found in the Data overview file of the Supporting Information). As a positive control for dimerization, we designed the "self-complementary" configuration AB1267DE345 (Figure 3, center), which was unable to fold intrastructurally and was therefore expected to preferentially dimerize at 3 M NaCl. Indeed, experimentally configuration AB1267DE345 displayed a measured dimeric assembly fraction of about 90%. In contrast to previous work utilizing other nonpolar modifications, we did not find any evidence for interstructure assembly that outcompeted intrastructure folding (if the latter was possible). This indicates that with our experimental conditions and sample concentrations used, intrastructure folding was strongly favored over dimerization.

2.3. Characterization of Rectangle Conformations

We went on to investigate the influence of the V40 configuration on "intrastructural" folding in greater detail. Peptides were either arranged in clusters (e.g., ABDE345) or in nonclustered configurations (e.g., AE1-7), which also included variations in the total number of V40 modifications. In order to classify the different folding states of the structures we used the aspect ratio r of the observed rectangles, which varied between $r = 0.3$ (for maximum overlap of the two leaves of the rectangle) and $r = 0.7$ (for a completely unfolded rectangle, further denoted
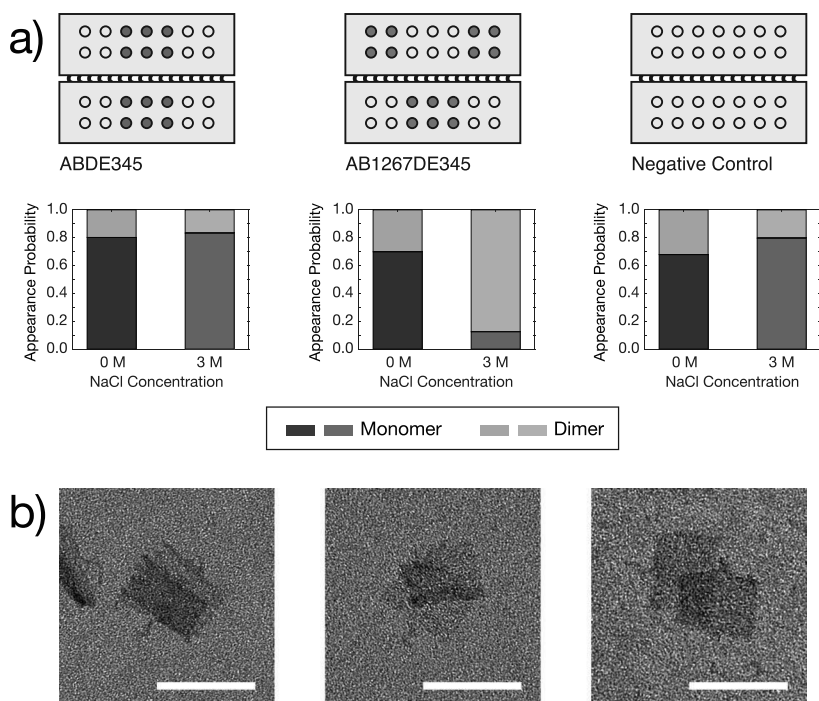
Figure 3. Statistics of dimeric rectangle assemblies. a) Distribution of monomers (dark colors) and dimers (light colors) for ABDE345, AB1267DE345 and the negative control. For 0 M NaCl (blue), the ELP is considered to be hydrophilic and the rectangle is open, while at 3 M NaCl (red) the ELPs are hydrophobic. b) Representative TEM images of dimeric DNA origami assemblies on the TEM grid for ABDE345. Scale bar: 100 nm.

as −F). The aspect ratio may therefore also be interpreted as a reaction coordinate for the folding process.

We quantified intrastructural folding for 14 different configurations by analyzing the probability distributions along the reaction coordinate r (**Figure** 4b; Data overview file, Supporting Information) using TEM imaging. Some of the configurations, e.g., BD1-7, did not fold at all and were only found in the −F state at 0 and 3 M NaCl. A second group of configurations predominantly populated states with mean aspect ratios of $r = 0.3$ and $r = 0.45$ (further denoted as +F0.3 and +F0.45, respectively). Only in a few cases aspect ratios between 0.45 and 0.7 were identified (further denoted as +Fx).

Figure 4b shows population densities $P(r)$ for six representative configurations along the reaction coordinate r for 0 M NaCl (blue) and 3 M NaCl (red). Even though the hinge of the rectangle was designed to promote folding of the structures into state +F0.3, the population densities of configurations ABDE1-7 and ABDE1267 show a global maximum for +F0.45 and only a local maximum for +F0.3. Furthermore, ABDE1-7 displayed folding even under nominally nonfolding conditions (0 M NaCl) and also populated the extreme +Fx states. This is consistent with the observation that in our fluorescence measurements ABDE1-7 showed the lowest T_t near room temperature (see **Figure** 5). In contrast, configuration ABDE345 populated mainly +F0.3 for 3 M NaCl with a smaller population at +F0.45. AE1-7 is the only nonclustered structure which we found capable of folding, and it mainly populated +F0.3 and less +F0.45. For its counterpart BD1-7—which has the same number of V40, but located directly next to the hinge—no folding was observed.

However, BD1-7 showed a large propensity for dimerization. A potential explanation for unfavorable intrastructural folding of BD1-7 could be the effect of steric hindrance between lines B and D, which would keep the hinge from completely closing. This would leave the ELPs partially exposed, which in turn would increase the relative energetic benefit of dimerization. The same rationale can be applied to AE1267 and its nonfolding counterpart BD1267 (see the Data overview file in the Supporting Information).

2.4. Hydrophobic Interactions and Folding Pathways

Quite generally, the creation of hydrophobic interfaces in water is energetically unfavorable, and such interfaces always "attempt" to minimize their interfacial energy. In the HP model, hydrophobic residues are located in the interior of a folded protein, where they are less exposed to polar molecules and where, most importantly, no bulk water exists. Accordingly, polar residues at the outside interact with the surrounding water molecules. Coacervates formed from collapsed ELPs usually have a high water content, but this "water of hydrophobic hydration" does not have the degrees of freedom of bulk water due to constraining H-bond interactions between the involved water molecules.[45] In fact, this water can be seen as part of the hydrophobic interface.

Although the twist of the structure was minimized in the design, we still expect a slight global twist. Since the origami rectangle structure is flexible and contains relatively thick adhesive peptide patches, it is conceivable that it will not exclusively fold through a rotation around its hinge. Therefore, we considered two plausible kinetic paths for folding of the structures (Figure 4c). First, the rectangle moves along the reaction coordinate and "searches" for its minimal energy state. Second, the rectangle closes around its hinge, reaches the +F0.3 state, and then starts searching for its minimal energy state. From the perspective of energy minimization by simply decreasing the exposed hydrophobic area and ideal ELP binding yield, +F0.3 should be the preferred state, because in the other states hydrophobic V40 would be still exposed to the surrounding aqueous solution.

2.5. Energetic Considerations

For a discussion of the overall conformation of the ELP rectangle, we may consider a planar molecular sheet modified with closely grafted peptides. Above T_t, where water is a poor solvent for the ELP, attractive interactions between the ELP chains due to van der Waals forces, solvation forces, etc., dominate over osmotic repulsion. Below T_t, with water as a good solvent, osmotic repulsion wins out due to the unfavorable entropy
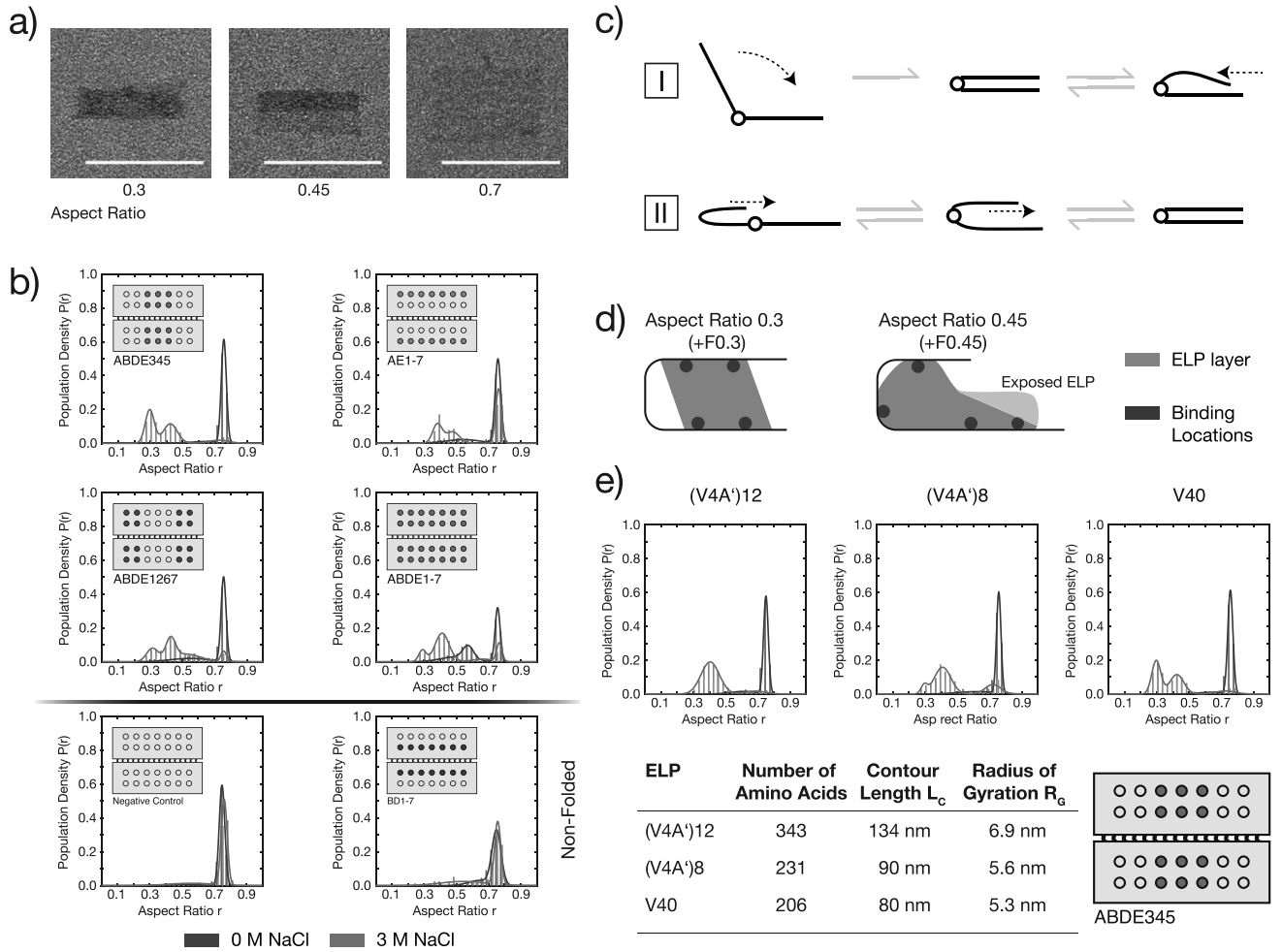
Figure 4. TEM analysis of the intramolecular rectangle folding. a) Representative TEM images for completely (+F0.3), partly (+F0.45), and nonfolded (−F) structures. Scale bar: 100 nm. b) Distributions of the measured aspect ratio for configurations ABDE345, AE1-7, ABDE1267, ABDE1-7, BD1-7, and the negative control at 0 M additional NaCl (blue) and 3 M additional NaCl (red). Insets illustrate the specific configuration. The distributions were fitted with Gaussian mixture functions (solid lines) with two, three, or four Gaussians where appropriate. c) Illustration of the two plausible kinetic paths. d) Illustration of hypothetic completely (+F0.3) and partly (+F0.45) folded rectangles. The ELP positions are shown as blue dots and the ELPs are represented by the red area. For +F0.45 the ELPs could partially exposed to surrounding water (light red area). e) Top: Distributions of the aspect ratio of ABDE345 for three different ELP variants (V4A')12, (V4A')8 and V40. The histograms are created according to the graphs in panel (b). Bottom: Corresponding number of amino acids, contour length, and radius of gyration for the peptides used.

penalty from chain compression.[46] Due to the complexity of the interactions it is difficult to estimate the dimensions of the peptides in their collapsed or noncollapsed phase, in particular when the conformation of an ELP in its collapsed form is a β-spiral. In order to gain an idea of the dimensions of the structure, we can roughly picture a single hydrophilic peptide as a random coil with a Kuhn segment length of 2.1 nm.[47] For V40, this results in a mean end-to-end distance of ≈ 13 nm and a radius of gyration of ≈ 5 nm (see Figure S8 in the Supporting Information). However, the distance between neighboring binding sites on the rectangle is ≈10–11 nm and the length of the double-stranded DNA (dsDNA) linker additionally adds ≈7.5 nm. Thus, the exploration volume of single L_{DNA}–V40 is larger than the distance between the binding sites. This alone could be a rationale for the measured rectangle states, where even a stretched conformation of ELPs is imaginable without being exposed to the surrounding water (see Figure 4d).

However, it has been shown[42] that the hydrophobic effect at the single peptide level can be well described by discriminating several contributions to the internal energy such as peptide–peptide, water–water, and peptide–water interactions. Depending on the system, these contributions can almost cancel each other, and thus the final internal energy becomes finally much smaller than the individual contributions. The more relevant free energy is much more puzzling since the entropy contributions cannot be discriminated so easily. Furthermore, the entropic nature of the ELP phase transition makes the collapse free energy strongly temperature sensitive. To get a better understanding of the system, approximations of effective interfacial energies or solvent–solute interactions could be used.[48] At the transition temperature, there is a balance between the collapsed and noncollapsed states. As the temperature increases, the entropic contribution becomes more important and results in the complete collapse of the
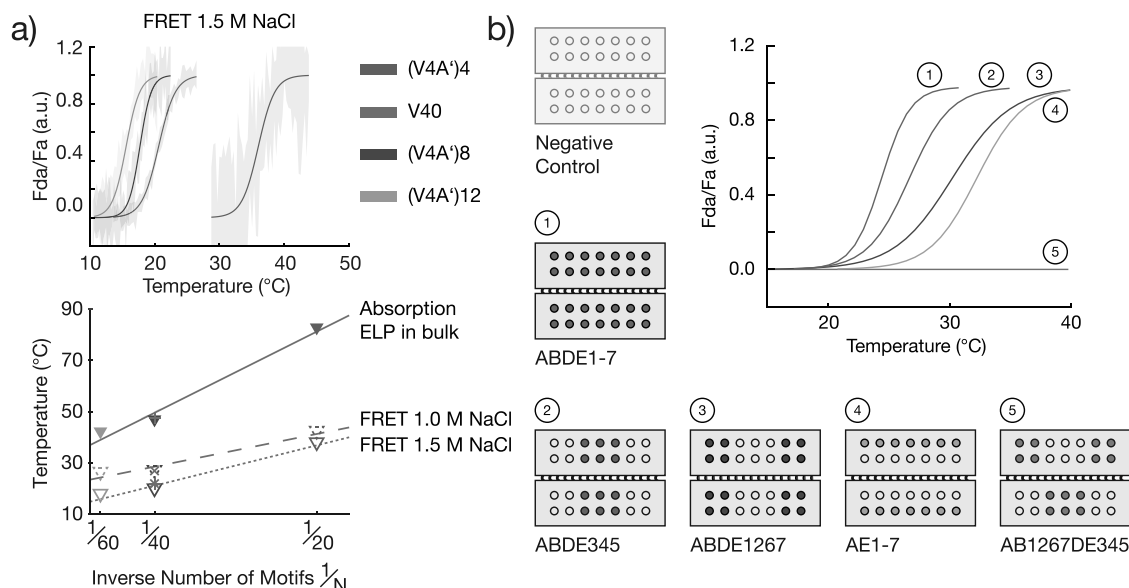
Figure 5. Analysis of the thermal folding of the rectangle ABDE345 using FRET. a) Top: Representative sigmoidal fits (solid lines) to averaged heating curves (not shown) of four different ELP variants (V4A')4 (purple), V40 (red), (V4A')8 (blue), and (V4A')12 (green) in 40×10^{-3} M Tris, 20×10^{-3} M acetate, 1×10^{-3} M EDTA, 20×10^{-3} M MgCl$_2$ and 1.5 M additional NaCl. The light-colored areas depict the standard deviations of each point of the averaged curves. Bottom: Transition temperatures T_t versus the inverse number of motifs of each ELP. T_t values were determined from sigmoidal fits to averaged heating curves. Triangles indicate noncanonic ELPs and red plus sign (no origami, bulk absorption, and no NaCl), red cross (origami, FRET 1 M NaCl), and red asterisk (origami, FRET 1.5 M NaCl) indicate the canonic V40. Filled symbols depict the T_t values of the ELP variants in bulk at a concentration of 25×10^{-6} M in 40×10^{-3} M Tris, 20×10^{-3} M acetate, 1×10^{-3} M EDTA, and 20×10^{-3} M MgCl$_2$. Hollow symbols depict the T_t values for the rectangles in 40×10^{-3} M Tris, 20×10^{-3} M acetate, 1×10^{-3} M EDTA, 20×10^{-3} M MgCl$_2$, and 1.0 M (dashed) resp. 1.5 M (solid) additional NaCl. As shown by the gray-colored fitting curves, the T_t values of the data sets scale with the inverse number of motifs $1/N$. b) Sigmoidal fits to normalized FRET data versus temperature of configurations ABDE1-7, ABDE345, ABDE1267, AE1-7, and AB1267DE345. For a better presentation, only the fit curves are shown. The data with fits can be found in the Data overview file in the Supporting Information.

ELP. For the ABDE345 configuration with six ELPs bound per leaf this would result in a total free energy change of about $\approx$800–1600 k_BT. It is surprising that almost identical values can be estimated only by looking at the interfacial energy change, which we estimated as $\approx$900-–1500 k_BT (see Section S2.7 in the Supporting Information). However, the latter picture would result in a non-negligible energy penalty of $\approx$150–250 k_BT per single ELP (see Section S2.7 in the Supporting Information) when it stays exposed to the surrounding water, which could be the case for the +F0.45 conformations. On the other hand, because of the relatively large exploration space of L$_{DNA}$–V40, in particular due to the relatively long linker, the hydrophobic ELPs could still be "buried" between the leaves and not exposed to water. Therefore, a simplified picture is not always useful, when multiple interactions are involved. Similar as in the discussion of the internal energy above, it is conceivable that small variations in one or two local parameters change the individual energy contributions to the hydrophobic effect quite drastically, but the total free energy does not.[42,49]

When the number of V40 and thus the size of the hydrophobic interface were reduced, for instance from ABDE1-7 to ABDE345, the state +F0.3 was more populated. Configurations ABDE1267 and AE1-7 vary only by one V40 per leaf in the case of perfect ELP binding yields. But due to the measured binding yields, a number difference of 1 should be negligible. Nevertheless, these two structures show quite different folding behavior. Furthermore, AE1-7 and BD1-7 exhibit the same interfacial area, but differ significantly in terms of infrastructure

dimerization. For that reason, a simple change of the peptide number or interfacial area cannot explain the measured distributions alone, pointing toward an intricate interplay of local concentration, ELP binding configuration, and conformation inside the peptide layer.

2.6. Influence of ELP Length

We also investigated the influence of ELP length on rectangle folding. To this end, we used four different ELPs with different contour lengths L_C and radii of gyration (see Figure 4e). The ELPs with the motif (V4A') are noncanonical ELPs with the canonical segment V4 = (GVGVP)$_4$ and A' as an alanine-rich peptide sequence (see Section S3 in the Supporting Information). Because of their length difference, they exhibit different bulk T_t, which scales with k/N, where k is a fit parameter (with Kelvin units) and N is the number of peptide motifs;[50,51] the latter can be canonical or noncanonical. Although V40 has a different amino acid composition than the noncanonical ELPs, its T_t also scales well with k/N (solid line in Figure 5a, bottom). Each of the different lengths was attached to the ABDE345 configuration, and the population distributions were determined for 0 and 3 M NaCl using TEM imaging (Figure 4e). As a result, we found that the longest ELP (V4A')12 only populates the +F0.45 state, but state +F0.3 gets more and more populated with decreasing radius of gyration. As expected, the rectangle with (V4A')4 did not exhibit any folding since the peptide's bulk

T_t was too high and 3 M NaCl was not sufficient to decrease the T_t to temperatures below room temperature. The observed transition from a favored +F0.45 to a favored +F0.3 due to a size change indicates that the peptides' exploration volume might be an important factor. With smaller ELPs, the rectangle is "forced" into the +F0.3 to prevent the exposure of ELPs to the surrounding water. But this would also imply a different ELP packing between the rectangle leaves and contributions from multiple interactions in the collapsed ELP phase.

2.7. Thermal Folding

In order to investigate the thermal behavior of the rectangles, we used ensemble fluorescence resonance energy transfer spectroscopy. As described above, the sample temperature was periodically changed, and the FRET signal of the incorporated dyes was used to report the conformational change of the rectangle. In this way, we were able to assess how the type of ELP used and their on-origami configuration influences the T_t of the ELP rectangle system. For +F0.3 the designed distance between the dyes is about 2.5 nm, and for +F0.45 this distance is in the range of about 17.5–22.5 nm and thus beyond the Förster radius. We therefore expected that the FRET signal mainly represents the occupation of the +F0.3 state.

The top graph in Figure 5a shows the normalized FRET signal versus sample temperature for the configuration ABDE345 for different ELPs, where the solid lines are sigmoidal fits to the data. It clearly shows that the specific T_t increases with decreasing contour length. Furthermore, the transition temperatures of the rectangle still scale with k/N (Figure 5a, bottom). It can also be seen that the slopes of the sigmoidal fits vary from peptide to peptide (Figure 5a, top). This effect is also found when the peptide is always V40, but its binding configuration is changed (Figure 5b). ABDE1-7 exhibits the lowest T_t, whereas ABDE345, ABDE1267, and AE1-7 exhibit increasing T_t values in that order, but with different slopes at T_t. Interestingly, a clear dependence on the "number" of V40 modifications was not found.

In bulk experiments, a change in the slope at transition indicates a cooperativity effect and usually decreases with increasing T_t.[51] As already discussed in more detail above, due to the random motion of the two leaves and their flexibility, it is plausible that during folding the two leaves initially contact each other only at one point, while other parts of the rectangle are still separated. For instance, configuration ABDE1267 consists of two clusters and during folding one cluster probably contacts its opposite cluster before the second does. This spatially confines the second cluster and decreases the entropy penalty for its collapse, which in turn gives rise to cooperative folding. Finally, the FRET measurements also hint toward an intimate coupling of multiple effects.

3. Conclusion

In this work, we generated a peptide-functionalized DNA origami-based macromolecular machine whose conformation can be reconfigured on demand through external stimuli. As the control mechanism, we used the fully reversible phase transition of elastin-like polypeptides, which allowed us to repeatedly switch the DNA structure's conformation by an alternating temperature cycle. Using Urry's classification this would be a zero-order molecular machine of the T_t type. The utilization of salt as stimulus for our device would classify it as a first-order molecular machine.

We also showed that the 2D arrangement of these ELPs on the rectangular structure used had a strong impact on its conformational states and thermodynamics. The results can be rationalized by adopting established principles for polymer and peptide folding, which point toward a balance between side chain and backbone interactions. In analogy to proteins, in our nanodevice, the DNA structure represents the backbone and the ELPs represent the side chains. The basic question in this context, and which is notoriously difficult to answer, is "what is the true balance between the different energetic contributions?." Our findings suggest that for the specific example of the ELP-modified rectangles a side-chain-centric rather than a backbone-centric view describes their overall behavior better, since the ELPs strongly determine the folding transition temperature. Structural details of the rectangular structure simply fine-tune the kinetics and thermodynamics of the folding process.

For future studies and potential applications of dynamic DNA devices, a variety of orthogonal tools and principles for design and fabrication are needed. In particular, other mechanical frameworks than DNA origami could be interesting, for instance protein-based filaments. The respond times of the structures might be reduced to the millisecond[52] or even microsecond range. A good stimulus candidate for the latter would be light.[53] The latter would also be a more sophisticated stimulus than salt for a first-order molecular machine of the T_t type. In this context, it would also be appealing to design a second-order molecular machine. Furthermore, applications in a biological context would make it necessary to utilize pH or biochemical stimuli,[37,38] e.g., phosphorylation and dephosphorylation, for a potential autonomous operation without external operator.

4. Experimental Section

lysis buffer per gram pellet and sonicated twice on ice for 9 min using 8 W with an interval of 10 s pulse and 20 s pause. The lysis buffer consisted of 1 mg mL^{-1} lysozyme, 1×10^{-3} M benzamidine, 1×10^{-3} M phenylmethylsulfonyl fluoride (PMSF) and 20 µL Turbo DNAse (Ambion ThermoFisher) in phosphate buffered saline (PBS). An aliquot of 1.5 mL 10% polyethyleneimine (PEI) in H$_2$O (2 mL per 1 L cell culture) was added and the lysate was distributed into 2 mL tubes. The tubes were heated to 60 °C for 10 min and then transferred back on ice. In the next step a "cold spin" was carried out, which consists of a centrifugation at 4 °C and 16 000 rcf for 10 min, after which the supernatant was transferred to new tubes. Crystalline NaCl was added and dissolved until the liquid turned turbid. The solution was centrifuged at room temperature at 16 000 rcf for 10 min and the supernatant was discarded; the preceding step was also called "hot spin." The pellets were resuspended in 500 µL PBS and a new cold spin was carried out. The series of cold and hot spins were repeated until no pellet was observed during the cold spin and the wanted volume was reached; usually, the series of cold and hot spins was repeated three times. The quality of the purification could be tested by running an 8–16% gradient sodium dodecyl sulfate-polyacrylamide gel electrophoresis (SDS-PAGE) for 35 min at 180 V. It is important to note that ELPs usually do not contain the amino acids, which are typically the target for commonly used stains, and thus the bands in the gel can be faint. Therefore, a negative stain with 0.5 M CuCl$_2$ or a positive silver stain were recommended. For testing, the final sample for contamination with other proteins a Coomassie stain is sufficient.

Conjugation of ELP to DNA: For the conjugation of ELPs to DNA, copper(I)-catalyzed alkyne–azide cycloaddition (further denoted as click chemistry) was used. ELPs were first activated with an azide group by using three types of bifunctional N-hydroxysuccinimide-azide (NHS-azide) linkers, namely NHS-C3-azide, NHS-PEG4-azide, and NHS-PEG12-azide, which were dissolved in dry dimethyl sulfoxide (DMSO). If not mentioned otherwise, NHS-C3-azide was used. The linkers were added in a fivefold to tenfold molar excess to the peptides provided in water or PBS. The reaction was incubated and shook for at least 6 h or overnight. Since the ELPs used do not have any free amines except for the N-terminus, side reactions on the peptide chains were not expected. The peptides were purified from unused linker by using centrifugal filters from Amicon with 10 kDa cutoff. For click chemistry, the alkyne-functionalized DNA (alkyne-TATGTAGATAATAGATGTATAA) was mixed with a threefold to fivefold molar excess of azide-ELP, ligand solution (100×10^{-6} M final solution; Tris[(1-benzyl-1H-1,2,3-triazol-4-yl)methyl]amine (TBTA) in DMSO; Tris[(1-hydroxypropyl-1H-1,2,3-triazol-4-yl)methyl]amine (THPTA) in H$_2$O; 2-(4-(((1-*tert*-butyl)-1H-1,2,3-triazol-4-yl)methl)amino)methyl-1H-1,2,3-triazol-1-yl)acetic acid) (BTTAA) in H$_2$O), CuSO$_4$ in H$_2$O (1×10^{-3} M final concentration), and fresh tris(2-carboxyethyl)phosphine (TCEP) (1×10^{-3} M final concentration). In the next step, the sample was incubated for 3 h or overnight at room temperature, and purified through salt precipitation. Therefore, 5 M NaCl in water was mixed with the sample in equal volumes and vortexed, which caused the solution to turn turbid. The solution was then centrifuged at 16 000 rcf at room temperature for 10 min. The supernatant was discarded and twofold distilled water or buffer was used to redissolve the pellet. The tube was cooled at 4 °C for 10 min and vortexed until the pellet vanished. The centrifugation and cooling steps were repeated twice for a sufficient purity.

DNA Origami Structure Assembly: The 7249 nucleotides (nt) long single-stranded "scaffold" strand from phage M13mp18[56] was folded into a twist-corrected rectangular DNA origami structure using about 200 short staple strands. These staple strands were used in a fourfold molar excess compared to the scaffold strand. As folding buffer (1× FB) 1× Tris-Acetat-EDTA buffer (40×10^{-3} M tris(hydroxymethyl)aminomethane (TRIS), 20×10^{-3} M acetate, 1×10^{-3} M EDTA) with 20×10^{-3} M MgCl$_2$ was used. For the folding of the structure an initial temperature of 70 °C for 3 min was used. The following temperature ramp started at 65 °C and ended with 45 °C after 1 h. Afterward, the solution was stored at 4 °C until further usage. The excess of unbound staples was removed by polyethylene glycol (PEG) precipitation according to Stahl et al.[57,58] Purification was carried out by adding an equal volume of 15% (w/v) PEG8000 in 1× FB with additional 505×10^{-3} M NaCl and vortexing for 30 s. Afterwards the

sample tube was centrifuged at 16 000 rcf and 20 °C for 30 min. The supernatant was carefully removed. The origami pellet was redissolved in the desired volume of 1× FB with additional 505×10^{-3} M NaCl and vortexed for 1 min. This purification step was repeated two more times. After the last purification the pellet was redissolved in 1× FB. Afterward the sample was incubated at room temperature over night or at 37 °C for at least 1 h. The concentration of the DNA rectangles was determined through absorption spectrometry (Nanophotometer IMPLEN vers. 7122V2.3.1, Munich, Germany) using an extinction coefficient of 1.12×10^8 M^{-1} cm^{-1}. To equip the rectangles with binding sites for ELP binding, specific staples were elongated by the sequence TTATACATCTATTATCTACATA, whose complementary sequence was conjugated to the ELPs. The rectangle was functionalized with these DNA–ELP constructs by adding them in a two to threefold molar excess (relative to the number of binding sites) to the origami solution. If necessary, the buffer solution was readjusted by adding 10× FB (400×10^{-3} M Tris, 200×10^{-3} M acetate 100×10^{-3} M EDTA 200×10^{-3} M MgCl$_2$). After the sample was incubated at room temperature for at least 1 h, it was purified right before further use with centrifugal filters from Amicon with a 10 kDa cutoff at 8000 rcf, at 4 °C for 10 min. The purification was repeated for three times.

Electrophoresis: To control the success of the peptide–DNA coupling, urea–PAGE (15%) was performed. About 4.8 g of urea, 1 mL of 10× TRIS-Borate-EDTA buffer (TBE), 3.75 mL of acrylamide (29:1), and 1.25 µL of H$_2$O were used in a total volume of 10 mL. To fully dissolve urea the solution was heated to 30–40 °C in an ultrasonic bath. The polymerization of the gel, before loading it in a preassembled gel cassette, was initiated by the addition of 28 µL 10% ammoniumpersulfate (APS) and 8 µL tetramethylethylenediamine. The samples were prepared with 2 µL gel loading buffer II and 0.5–1 µL peptide–DNA sample, and were denatured through heating to 95 °C for 5 min. Before the denatured peptide–DNA samples were loaded, the gel chamber was incubated with 1× TBE at 60 °C using a connected water bath for half an hour; furthermore, a voltage of 40 V was applied to the geld. Electrophoresis was carried out using 100 V at 60 °C for 60 to 75 min, followed by staining with SYBR Gold Nucleic Acid Gel stain (ThermoFisher Scientific) and visualized using UV light.

Atomic Force Microscopy: For AFM imaging, 5 µL of 5×10^{-9} M origami sample in 1× FB was deposited onto freshly cleaved mica. After an incubation of 5 min, 60 µL of the same buffer was added. An Asylum Research Cypher Scanning Probe Microscope was used in tapping mode with the Asylum Research environmental scanner. The silicon cantilever (Olympus micro-cantilevers BL-AC40TS-C2) had a nominal force constant of 0.09 N m^{-1} and a resonance frequency in water of 25 kHz. The scan rate was between 1 and 4 Hz. The AFM software was implemented in Igor pro 6.34 A. Image processing was performed with ImageJ.

Transmission Electron Microscopy: The staining solution was freshly prepared by adding 1 µL of 5 M NaOH to 200 µL 2% (w/v) uranyl formate in water and vortexing it for 1 min. To sediment the large unwanted uranyl crystals, which would be seen as black spots on the grid, the solution was centrifuged for 5 min at 20 000 rcf at 4 °C. The sample was prepared in 5×10^{-9} M concentration in 1× FB with an optional addition of 3 M NaCl. For the positive stain, 5 µL of the sample was put on a grid (FCF-400-Cu Formvar Carbon Film 400 Mesh grid from Electron Microscopy Sciences) and incubated for 30 s. The excess of liquid was removed by a filter paper and the grid was washed with 5 µL of the staining solution. An aliquot of 20 µL of staining solution was added, and the grid was incubated for 60 s, before the drop was removed. The grid was washed by dipping it three times in a drop of water and the excess was removed with a filter paper. The finished grid was dried for 20 min in air or in a desiccator. The prepared samples were imaged using a Philipps CM100 transmission electron microscope at 100 kV.

FRET Experiments: The FRET experiments were performed using the CARY Eclipse Fluorescence Spectrometer from Varian Inc. The microcuvettes were cleaned with H$_2$O, 70% ethanol, and water, before drying with a stream of air. The cuvettes were passivated by incubating the sample chamber in 1% (w/v) bovine serum albumin for 10 min at room temperature. The cuvettes were then washed with pure water and

dried with a stream of air. To prevent evaporation and therefore a change in solution properties, 600 µL of *n*-hexadecane was added on top of the samples. The sample contained 30 µL origami-ELP solution in 1× FB and 30 µL of the same buffer solution with additional 2 M NaCl resulting in a final concentration of 1 M NaCl. The measurements were carried out by repeated heating and cooling ramps from 10 to 55 °C with a rate of 0.5 °C min^{-1} and a lag time of 2 min between each ramp; at least five heating and cooling ramps were measured. The dyes used were ATTO 532 (excitation λ_{Ex} = 530 nm; emission λ_{Em} = 550 nm) and ATTO 647N (excitation λ_{Ex} = 645 nm; emission λ_{Em} = 665 nm). Throughout this work, the presented temperature profiles of the various rectangle variants were always averaged temperature profiles with a mean T_t.

Absorption Measurements: The absorption measurements were carried out at a fixed wavelength of 280 nm using a Jasco J-815 CD-Spectrometer (a combined CD and UV–vis spectrometer) equipped with a peltier cuvette holder. All ELPs were dissolved in 1× FB and had a concentration of 25×10^{-6} M to compare the T_t of the ELP variants. To examine the influence of V40 concentration on T_t, concentrations of 1×10^{-6}, 5×10^{-6}, and 10×10^{-6} M, were used with the aforementioned buffer with additional 1 M NaCl. Initially, the sample temperature was changed between 10 to 80 °C with a rate of 2 °C min^{-1} to roughly determine the T_t. Finally, the temperature range was set around the specific T_t of each sample and measured with a rate of 0.5 °C min^{-1}. Heating and cooling curves were measured to observe the typical hysteresis as well.

Supporting Information

Supporting Information is available from the Wiley Online Library or from the author.

Acknowledgements

Conflict of Interest

The authors declare no conflict of interest.

Keywords

[1] V. Balzani, A. Credi, M. Venturi, *Molecular Devices and Machines*, Wiley-VCH Verlag GmbH & Co. KGaA, Weinheim, Germany **2008**.
[2] P. W. K. Rothemund, *Nature* **2006**, *440*, 297.
[3] H. Dietz, S. M. Douglas, W. M. Shih, *Science* **2009**, *325*, 725.
[4] A. Kuzyk, R. Schreiber, Z. Fan, G. Pardatscher, E.-M. Roller, A. Högele, F. C. Simmel, A. O. Govorov, T. Liedl, *Nature* **2012**, *483*, 311.
[5] J. J. Funke, H. Dietz, *Nat. Nanotechnol.* **2016**, *11*, 47.
[6] P. C. Nickels, B. Wünsch, P. Holzmeister, W. Bae, L. M. Kneer, D. Grohmann, P. Tinnefeld, T. Liedl, *Science* **2016**, *354*, 305.
[7] M. Endo, H. Sugiyama, *Molecules* **2018**, *23*, 11751.
[8] A. E. Marras, L. Zhou, H.-J. Su, C. E. Castro, *Proc. Natl. Acad. Sci. USA* **2015**, *112*, 713.
[9] A. E. Marras, Z. Shi, M. G. Lindell, R. A. Patton, C.-M. Huang, L. Zhou, H.-J. Su, G. Arya, C. E. Castro, *ACS Nano* **2018**, *12*, 9484.
[10] J. List, M. Weber, F. C. Simmel, *Angew. Chem., Int. Ed.* **2014**, *53*, 4236.
[11] J. List, M. Weber, F. C. Simmel, *Angew. Chem.* **2014**, *126*, 4321.
[12] T. Gerling, K. F. Wagenbauer, A. M. Neuner, H. Dietz, *Science* **2015**, *347*, 1446.
[13] V. A. Turek, R. Chikkaraddy, S. Cormier, B. Stockham, T. Ding, U. F. Keyser, J. J. Baumberg, *Adv. Funct. Mater.* **2018**, *28*, 1706410.
[14] A. Kuzyk, R. Schreiber, H. Zhang, A. O. Govorov, T. Liedl, N. Liu, *Nat. Mater.* **2014**, *13*, 862.
[15] F. C. Simmel, B. Yurke, H. R. Singh, *Chem. Rev.* **2019**, *119*, 6326.
[16] S. M. Douglas, I. Bachelet, G. M. Church, *Science* **2012**, *335*, 831.
[17] K. Vogele, J. List, G. Pardatscher, N. B. Holland, F. C. Simmel, T. Pirzer, *ACS Nano* **2016**, *10*, 11377.
[18] S. Hernández-Ainsa, K. Misiunas, V. V. Thacker, E. A. Hemmig, U. F. Keyser, *Nano Lett.* **2014**, *14*, 1270.
[19] E. Kopperger, J. List, S. Madhira, F. Rothfischer, D. C. Lamb, F. C. Simmel, *Science* **2018**, *359*, 296.
[20] A. M. Maier, C. Weig, P. Oswald, E. Frey, P. Fischer, T. Liedl, *Nano Lett.* **2016**, *16*, 906.
[21] S. Lauback, K. R. Mattioli, A. E. Marras, M. Armstrong, T. P. Rudibaugh, R. Sooryakumar, C. E. Castro, *Nat. Commun.* **2018**, *9*, 1446.
[22] Y. Kamiya, H. Asanuma, *Acc. Chem. Res.* **2014**, *47*, 1663.
[23] A. Kuzyk, Y. Yang, X. Duan, S. Stoll, A. O. Govorov, H. Sugiyama, M. Endo, N. Liu, *Nat. Commun.* **2016**, *7*, 10591.
[24] C. K. McLaughlin, G. D. Hamblin, H. F. Sleiman, *Chem. Soc. Rev.* **2011**, *40*, 5647.
[25] A. A. Greschner, V. Toader, H. F. Sleiman, *J. Am. Chem. Soc.* **2012**, *134*, 14382.
[26] T. G. W. Edwardson, K. M. M. Carneiro, C. K. McLaughlin, C. J. Serpell, H. F. Sleiman, *Nat. Chem.* **2013**, *5*, 868.
[27] Y. Y. Zhang, C. Wang, Y. C. Dong, D. M. Wang, T. Y. Cao, S. Wang, D. S. Liu, *Adv. Funct. Mater.* **2019**, *29*, 1809097.
[28] F. A. Aldaye, H. F. Sleiman, *J. Am. Chem. Soc.* **2007**, *129*, 13376.
[29] R. P. Goodman, M. Heilemann, S. Doose, C. M. Erben, A. N. Kapanidis, A. J. Turberfield, *Nat. Nanotechnol.* **2008**, *3*, 93.
[30] E. S. Andersen, M. Dong, M. M. Nielsen, K. Jahn, R. Subramani, W. Mamdouh, M. M. Golas, B. Sander, H. Stark, C. L. P. Oliviera, J. S. Pedersen, V. Birkedal, F. Besenbacher, K. V. Gothelf, J. Kjems, *Nature* **2009**, *459*, 73.
[31] A. S. Walsh, H. Yin, C. M. Erben, M. J. A. Wood, A. J. Turberfield, *ACS Nano* **2011**, *5*, 5427.
[32] A. Banerjee, D. Bhatia, A. Saminathan, S. Chakraborty, S. Kar, Y. Krishnan, *Angew. Chem. Int. Ed.* **2013**, *52*, 6854.
[33] A. Banerjee, D. Bhatia, A. Saminathan, S. Chakraborty, S. Kar, Y. Krishnan, *Angew. Chem.* **2013**, *125*, 6992.
[34] D. W. Urry, *J. Phys. Chem. B* **1997**, *101*, 11007.
[35] R. L. DiMarco, S. C. Heilshorn, *Adv. Mater.* **2012**, *24*, 3923.
[36] S. Hollingshead, C.-Y. Lin, J. C. Liu, *Macromol. Biosci.* **2017**, *17*, 1600554.
[37] D. W. Urry, *Angew. Chem., Int. Ed. Engl.* **1993**, *32*, 819.
[38] D. W. Urry, *Angew. Chem.* **1993**, *105*, 859.
[39] E. E. Meyer, K. J. Rosenberg, J. N. Israelachvili, *Proc. Natl. Acad. Sci. USA* **2006**, *103*, 15739.

[40] K. A. Dill, S. Bromberg, K. Yue, K. M. Fiebig, D. P. Yee, P. D. Thomas, H. S. Chan, *Protein Sci.* **1995**, *4*, 561.

[41] K. A. Dill, *Protein Sci.* **1999**, *8*, 1166.

[42] D. Horinek, A. Serr, M. Geisler, T. Pirzer, U. Slotta, S. Q. Lud, J. A. Garrido, T. Scheibel, T. Hugel, R. R. Netz, *Proc. Natl. Acad. Sci. USA* **2008**, *105*, 2842.

[43] S. Sagredo, T. Pirzer, A. Aghebat Rafat, M. A. Goetzfried, G. Moncalián, F. C. Simmel, F. de la Cruz, *Angew. Chem., Int. Ed.* **2016**, *55*, 4348.

[44] S. Sagredo, T. Pirzer, A. Aghebat Rafat, M. A. Goetzfried, G. Moncalián, F. C. Simmel, F. de la Cruz, *Angew. Chem.* **2016**, *128*, 4421.

[45] D. W. Urry, S. Q. Peng, J. Xu, D. T. McPherson, *J. Am. Chem. Soc.* **1997**, *119*, 1161.

[46] J. N. Isreaelachvili, *Intermolecular and Surface Forces*, Academic Press, London **1997**.

[47] S. Fluegel, K. Fischer, J. R. McDaniel, A. Chilkoti, M. Schmidt, *Biomacromolecules* **2010**, *11*, 3216.

[48] M. Levitt, R. Sharon, *Proc. Natl. Acad. Sci. USA* **1988**, *85*, 7557.

[49] T. Pirzer, T. Hugel, *ChemPhysChem* **2009**, *10*, 2795.

[50] D. E. Meyer, A. Chilkoti, *Biomacromolecules* **2004**, *5*, 846.

[51] A. Ghoorchian, N. B. Holland, *Biomacromolecules* **2011**, *12*, 4022.

[52] L. K. Bruetzel, P. U. Walker, T. Gerling, H. Dietz, J. Lipfert, *Nano Lett.* **2018**, *18*, 2672.

[53] J. Raphel, A. Parisi-Amon, S. Heilshorn, *J. Mater. Chem.* **2012**, *22*, 19429.

[54] A. Ghoorchian, J. T. Cole, N. B. Holland, *Macromolecules* **2010**, *43*, 4340.

[55] S. R. MacEwan, W. Hassouneh, A. Chilkoti, *J. Vis. Exp.* **2014**, *88*, e51583.

[56] B. Kick, F. Praetorius, H. Dietz, D. Weuster-Botz, *Nano Lett.* **2015**, *15*, 4672.

[57] E. Stahl, T. G. Martin, F. Praetorius, H. Dietz, *Angew. Chem., Int. Ed.* **2014**, *53*, 12735.

[58] E. Stahl, T. G. Martin, F. Praetorius, H. Dietz, *Angew. Chem.* **2014**, *126*, 12949.